$K^-d \to \pi\Lambda N$ reaction for studying charge symmetry breaking in the ΛN interaction

Yutaro Iizawa [*] and Daisuke Jido
Department of Physics, Tokyo Institute of Technology, 2-12-1 Ookayama, Megro, Tokyo 152-8551, Japan

Takatsugu Ishikawa
Research Center for Electron Photon Science (ELPH), Tohoku University, Sendai 982-0826, Japan

(Received 17 January 2022; revised 17 July 2022; accepted 26 September 2022; published 13 October 2022)

We propose to utilize the $K^-d \to \pi^-\Lambda p$ and $K^-d \to \pi^0\Lambda n$ reactions in order to investigate the difference between the low-energy Λp and Λn interactions. In these reactions, the Λp and Λn scatterings appear as final state interactions. We calculate the differential cross sections of these reactions with stopped kaons theoretically. We introduce isospin breaking by using the physical masses for the participating hadrons and through the chiral unitary amplitudes for $K^-N \to \pi N$ and $K^-N \to \bar{K}N$. With stopped kaons, the ΛN interaction takes place dominantly in the spin-triplet state thanks to the deuteron spin and s-wave dominance of the scattering amplitudes at low energy. We find that the ratio of the ΛN invariant mass spectra of these reactions is useful for revealing qualitative properties of charge symmetry breaking in the low-energy ΛN interaction. We also find that the contributions coming from the π and Σ exchange diagrams which have πN final state interaction and $\Sigma N \to \Lambda N$ conversion, respectively, are negligibly small around the ΛN threshold, while the contributions from the impulse diagram without final state interactions and the $\bar{K}$ exchange diagram containing the $\pi\Lambda$ final state interaction are main sources of the background.

DOI: 10.1103/PhysRevC.106.045201

I. INTRODUCTION

Charge symmetry breaking in the ΛN system appears as a difference between the Λp and Λn interactions, and is caused by the isospin symmetry breaking. Recently a large isospin symmetry breaking effect has been suggested by experimental analysis for the $A = 4$ mirror hypernuclei [1,2]. From the experimental data, one finds that the excitation energies of the first 1^- states are different by 0.3 MeV between ${}^4_\Lambda$H and ${}^4_\Lambda$He (both the ground states are 0^+), while the difference between nuclear systems ^{3}H and ^{3}He is just 0.071 MeV after correcting for electromagnetic effects [3]. Therefore, one expects a large difference between the Λp and Λn interactions. The scattering length $a_{\Lambda p}$ and effective range $r_{\Lambda p}$ for Λp scattering were determined experimentally by analyzing the Λp final state interaction in the $pp \to K^+\Lambda p$ reaction [4] and their values were extracted as $a^s_{\Lambda p} = -2.43^{+0.16}_{-0.25}$ fm and $r^s_{\Lambda p} = 2.21^{+0.16}_{-0.36}$ fm for the spin-singlet channel, and $a^t_{\Lambda p} = -1.56^{+0.19}_{-0.22}$ fm and $r^t_{\Lambda p} = 3.7^{+0.6}_{-0.6}$ fm for the spin-triplet channel. Here we use the sign convention as positive (negative) scattering length for repulsive (attractive) interaction. On the other hand, the low-energy Λn scattering parameters have not been experimentally determined yet. Therefore it is necessary to confirm whether charge symmetry breaking in the ΛN interaction is large, and it is important to know the direction of charge symmetry breaking.

For theoretical approaches, several phenomenological investigations of the ΛN interaction have been performed by using boson-exchange models (Nijmegen [5–7], Jülich [8–10] and Ehime [11,12]), quark models [13–15], and hybrid model known as Kyoto-Niigata [16]. Effective field theory approaches have also investigated the ΛN interactions based on the SU(3) chiral symmetry [17–27]. Among them isospin symmetry breaking in the ΛN interactions was investigated in Ref. [27], giving a difference of the ΛN scattering lengths $\Delta a^{\rm CSB} \equiv a_{\Lambda p} - a_{\Lambda n}$ of 0.62 ± 0.08 fm for the spin-singlet state and -0.10 ± 0.02 fm for the spin-triplet state.

In this paper, we propose the $K^-d \to \pi\Lambda N$ reaction with stopped kaons in order to study the direction of charge symmetry breaking in the ΛN interaction from the final state interactions. One of the advantages of the reaction is that it is initiated by the same K^-d system and includes $\pi^-\Lambda p$ and $\pi^0\Lambda n$ in the final states, which are isospin partners. Thus, we can use the same theoretical framework for these two final states and the formulation can be fixed by better-known Λp channel to apply the uncertain Λn channel. By taking the cross section ratio of these two final states, we can study how the isospin symmetry breaking effects appear in the scattering parameters of the ΛN interaction. The spin of the ΛN system is either singlet or triplet. If one considers stopped kaons, the spin-triplet configuration dominates the ΛN final state interaction around its production threshold because the deuteron has spin 1 and the non-spin-flip s-wave interactions are the main contributions at low energies. This is a good feature to fix the spin configuration of the ΛN system. It is also reported in Refs. [28,29] that, thanks to the finite size of the deuteron,

[*] iizawa.y.aa@m.titech.ac.jp

 ©2022 American Physical Society

K^- in the atomic p-orbit is also absorbed by the s-wave K^-N interaction.

Historically the $K^-d \to \pi^-\Lambda p$ reaction has been studied to investigate the Λp scattering and also the ΣN interaction with kaons at rest [30,31] and in flight [32–35]. There are many theoretical calculations of this reaction with kaons at rest so far [28,36–46]. Some of these works have mainly concerned a possible bound state below the ΣN threshold by considering Σ-Λ conversion in the intermediate states. Here, focusing on the Λp and Λn interactions, we revisit this reaction based on the formulation developed in Refs. [47–50] by using modern meson-baryon $\bar{K}N \to MB$ scattering amplitudes obtained by the chiral unitary approach [51–57] and introducing isospin breaking in the ΛN interaction and the scattering amplitudes. The chiral unitary amplitudes have isospin symmetry breaking introduced by using the physical masses in the loop functions and reproduce the observed cross sections of K^-p to various channels, say $\pi^-\Sigma^+$ and $\pi^+\Sigma^-$, at low energies. We include the kaon rescattering diagram together with the quasifree production of the Λ hyperon, which are main sources of the background.

The structure of this paper is as follows. In Sec. II, we explain our theoretical formalism to calculate the $K^-d \to \pi\Lambda N$ reactions. In Sec. III we show our numerical results and discuss the effects of isospin symmetry breaking in the ΛN interaction. Section IV is devoted to the summary and conclusion.

II. FORMULATION

A. Kinematics

The reaction $K^-d \to \pi\Lambda N$ requires five kinematical variables to fix the phase space of the three-body final state [58]. In this study we are interested in the mass spectra of the ΛN systems, thus we choose the following variables for unpolarized deuteron targets: the ΛN invariant mass $M_{\Lambda N}$, the solid angle of the final pion in the total center-of-mass (c.m.) frame Ω_π, and the solid angle of the final Λ in the Λ-nucleon c.m. frame Ω^*_Λ. Considering stopped kaons, a reference of the coordinate is taken along the direction of the final-pion emission. In addition, once one fixes the reaction plane, the scattering amplitude does not depend on the azimuthal angle of Ω^*_Λ for unpolarized deuterons. The cross section of the reaction is calculated by

$$d\sigma = \frac{1}{(2\pi)^3}\frac{M_d M_\Lambda M_N}{2k_{\rm c.m.}E^2_{\rm c.m.}}|\mathcal{T}|^2|\boldsymbol{p}_\pi|\,|\boldsymbol{p}^*_\Lambda|\,dM_{\Lambda N}d\cos\theta^*_\Lambda, \quad (1)$$

where $E_{\rm c.m.}$ is the total c.m. energy, $k_{\rm c.m.}$ and $\boldsymbol{p}_\pi$ are the initial K^- and final π momenta in the total c.m. frame, respectively, $\boldsymbol{p}^*_\Lambda$ and θ^*_Λ denote the momentum and the polar angle of the final Λ in the Λ-nucleon c.m. frame, respectively, and $\mathcal{T}$ represents the T matrix of the reaction.

B. K^-d scattering amplitudes

In this section, we formulate the scattering amplitudes of the $K^-d \to \pi\Lambda N$ reactions by following Refs. [47–50]. The Feynman diagrams that we consider in our calculation are given in Fig. 1 for the Λp process and Fig. 2 for the Λn process. The initial K^- is absorbed by one of the nucleons in the deuteron as $K^-N \to \pi Y$ or $K^-N \to \bar{K}N$. In Dia. 1, the Λ hyperon produced by the K^- absorption scatters with another nucleon. This diagram, which we call the Λ exchange diagram, is our target diagram (foreground) that contains the final state interaction of ΛN. Diagram 2 has the Σ hyperon exchange and contains a transition amplitude of $\Sigma N \to \Lambda N$. In Dia. 3, which we call impulse approximation, the K^- absorption takes place without any final state interaction. In Dia. 4 the initial K^- scatters with one of the nucleons in the deuteron and rescatters with another nucleon. We call this diagram K exchange. Diagrams 3 and 4 will turn out to be main sources of the background. Diagram 5 has the pion exchange with final state interaction between a pion and a nucleon. We will see later that the pion exchange contribution is negligibly small.

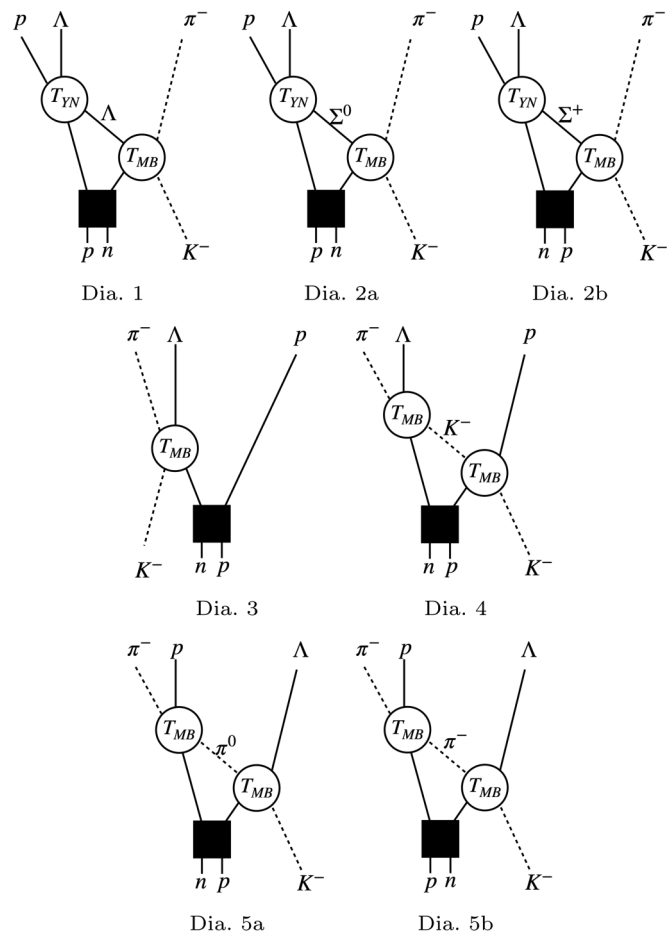

FIG. 1. Feynman diagrams used for the calculation of the Λp process. In the diagrams, T_{MB} (T_{YN}) denotes the meson-baryon (hyperon-nucleon) amplitude scattering amplitude.

The c.m. energies of these processes are low enough and one may use s-wave amplitudes. We use the hadron masses given in the Review of Particle Physics [58] in the following calculation.

First, we formulate the amplitude of the Λ exchange diagrams Dia. 1 in Figs. 1 and 2. According to Ref. [48], we can

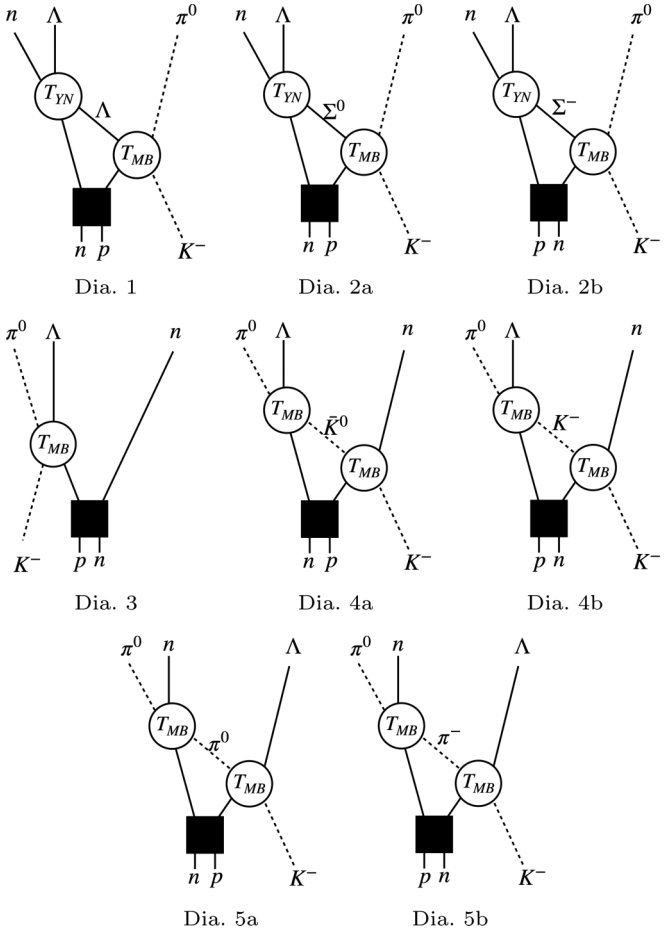

FIG. 2. Same as in Fig. 1 but for the Λn process.

write the scattering amplitude for the Λ exchange diagram as

$$\mathcal{T}^{(1)}_{\pi\Lambda N} = T_{\Lambda N}(M_{\Lambda N}) \int \frac{d^3q}{(2\pi)^3} \frac{2M_\Lambda}{q^2 - {M_\Lambda}^2 + i\epsilon} \times \tilde{\varphi}(\boldsymbol{q} + \boldsymbol{p}_\pi)\, T_{K^-N\to\pi\Lambda}(W) \tag{2}$$

where $M_{\Lambda N}$ is the invariant mass of Λ and N in the final state, q is the momentum of the exchange Λ, $\tilde{\varphi}$ is the s-wave deuteron wave function in the momentum space, and W denotes the invariant mass of the initial kaon and the nucleon inside the deuteron. The amplitudes $T_{\Lambda N}$ and $T_{K^-N\to\pi\Lambda}$ stand for the s-wave scattering amplitudes of the $\Lambda N \to \Lambda N$ and $K^-N \to \pi\Lambda$ processes, respectively. The charges of N and π are fixed in each process as shown in Figs. 1 and 2. For instance, $K^-N \to \pi\Lambda$ for the Λp process corresponds to $K^-n \to \pi^-\Lambda$.

The nonrelativistic propagator is extended to a relativistic one as

$$\frac{1}{q_0 - \sqrt{\boldsymbol{q}^2 + M^2} + i\epsilon} \simeq \frac{2M}{q^2 - M^2 + i\epsilon}$$

for simplicity of the calculation. With this approximation we can perform the momentum integral of Eq. (2) analytically, which reduces the calculation costs a lot.

For the baryon exchange diagrams, q^0 and W are fixed as

$$q^0 = M_{K^-} + M_d - \left(M_2 - \frac{B_d}{2}\right) - p^0_\pi, \tag{3}$$

$$W = \left(M_1 - \frac{B_d}{2}\right) + M_{K^-}, \tag{4}$$

where B_d is the binding energy of a deuteron, M_1 (M_2) is the participant (spectator) nucleon mass in $K^-N \to \pi\Lambda$, and p^0_π is the energy of the final state pion.

We neglect the small d-wave component of the deuteron wave function and use a parametrization of the s-wave component given by an analytic function in the CD-Bonn potential [59] as

$$\tilde{\varphi}(p) = N \sum_{j=1}^{11} \frac{C_j}{p^2 + m_j^2}, \tag{5}$$

where N is the normalization factor, and C_j and m_j were determined in Ref. [59]. The argument of $\tilde{\varphi}$ in Eq. (2) is fixed by the momentum conservation of the vertex of the first scattering.

Next, the Σ exchange diagrams given by Dia. 2 in Figs. 1 and 2 are formulated as

$$\mathcal{T}^{(2)}_{\pi\Lambda N} = T_{\Sigma N\to\Lambda N}(M_{\Lambda N}) \int \frac{d^3q}{(2\pi)^3} \frac{2M_\Sigma}{q^2 - {M_\Sigma}^2 + i\epsilon} \times \tilde{\varphi}(\boldsymbol{q} + \boldsymbol{p}_\pi)\, T_{K^-N\to\pi\Sigma}(W) \tag{6}$$

as well as the foreground diagram. Here q_0 and W are fixed as we do in Eqs. (3) and (4). The charge of the exchange Σ is specified in Figs. 1 and 2.

Then we consider the amplitudes of the impulse approximation given by Dia. 3. The amplitudes are calculated as

$$\mathcal{T}^{(3)}_{\pi\Lambda N} = T_{K^-N\to\pi\Lambda}(M_{\pi\Lambda})\, \tilde{\varphi}(\boldsymbol{p}_N), \tag{7}$$

where $\boldsymbol{p}_N$ is the momentum of the spectator nucleon in the rest frame of the deuteron.

The kaon exchange processes given by Dia. 4 can be calculated as

$$\mathcal{T}^{(4)}_{\pi\Lambda N} = T_{\bar{K}N\to\pi\Lambda}(M_{\pi\Lambda}) \int \frac{d^3q}{(2\pi)^3} \frac{\tilde{\varphi}(\boldsymbol{q} + \boldsymbol{p}_N)}{q^2 - M_{\bar{K}}^2 + i\epsilon} \times T_{K^-N\to\bar{K}N}(W). \tag{8}$$

For $K^-d \to \pi^-\Lambda p$, the exchanged kaon is only K^-, however for $K^-d \to \pi^0\Lambda n$, K^- and $\bar{K}^0$ are allowed as the exchanged kaon considering charge conversion. For the kaon exchange diagrams, q^0 is fixed as

$$q^0 = M_{K^-} + M_d - \left(M_2 - \frac{B_d}{2}\right) - p^0_N \tag{9}$$

with p^0_N the energy of the final state nucleon and W is the same as Eq. (4).

Finally we obtain the amplitudes for the pion exchange processes given by Dia. 5 as

$$\mathcal{T}^{(5)}_{\pi\Lambda N} = T_{\pi N\to\pi N}(M_{\pi N}) \int \frac{d^3q}{(2\pi)^3} \frac{\tilde{\varphi}(\boldsymbol{q} + \boldsymbol{p}_\Lambda)}{q^2 - M_\pi^2 + i\epsilon} \times T_{K^-N\to\pi\Lambda}(W), \tag{10}$$

where both π^0 and π^- are allowed as the exchanged pion for each process, and $\boldsymbol{p}_\Lambda$ is the momentum of the final state Λ baryon in the total c.m. frame. For the pion exchange diagrams, q^0 is fixed as

$$q^0 = M_{K^-} + M_d - \left(M_2 - \frac{B_d}{2}\right) - p^0_\Lambda \tag{11}$$

with p^0_Λ the energy of the final state Λ baryon and W is the same as Eq. (4).

The total amplitude for $K^-d \to \pi\Lambda N$ is given by the sum of all amplitudes described above as

$$\mathcal{T}_{\pi\Lambda N} = \sum_j \mathcal{T}^{(j)}_{\pi\Lambda N}. \tag{12}$$

The amplitude of primary interest (the foreground amplitude) in our calculation for $K^-d \to \pi\Lambda N$ is given by the Λ exchange diagram (Dia. 1 in Figs. 1 and 2) as

$$\mathcal{T}^{\rm FG}_{\pi\Lambda N} = \mathcal{T}^{(1)}_{\pi\Lambda N}, \tag{13}$$

and we call the rest of the processes background,

$$\mathcal{T}^{\rm BG}_{\pi\Lambda N} = \sum_{j\neq 1} \mathcal{T}^{(j)}_{\pi\Lambda N}. \tag{14}$$

The relative phases of these amplitudes are safely fixed within the model. As discussed in the next subsection, the meson-baryon scattering amplitudes are calculated by using the chiral unitary approach in which the amplitudes are obtained by resumming the interaction kernel given by the chiral perturbation theory. The interaction kernels are obtained at the tree level, having real values. The baryon-baryon interactions are parametrized by the effective range expansion and the values at the threshold are given by the scattering length which is real for the ΛN interaction. In this way the phases of the two-body amplitudes are fixed without any ambiguities.

The isospin breaking effects on the T matrix of the reaction $\mathcal{T}$ are counted by using the observed masses for the exchanged particles and through the amplitudes of the absorption processes and the final state interactions. The details of isospin breaking of these amplitudes are described below.

C. Hyperon-nucleon and meson-baryon amplitudes

In this section, we explain the hyperon-nucleon and meson-baryon amplitudes that we use in the calculation of the cross section. We parametrize the low-energy s-wave ΛN scattering amplitude by the scattering length $a_{\Lambda N}$ and the effective range $r_{\Lambda N}$ given by

$$T_{\Lambda N} = \mathcal{N}\frac{1}{-\dfrac{1}{a_{\Lambda N}} + \dfrac{1}{2}r_{\Lambda N}p^{*2}_\Lambda - ip^*_\Lambda}, \tag{15}$$

where p^*_Λ is the momentum in the Λ-nucleon c.m. frame, and the kinematic factor $\mathcal{N}$ is given by

$$\mathcal{N} = -\frac{8\pi M_{\Lambda N}}{\sqrt{(2M_Y)(2M_2)(2M_f)(2M_\Lambda)}} \tag{16}$$

for the $YN_2 \to \Lambda N_f$ process, where M_Y, M_2 and M_f are the masses of Y, N_2, and N_f, respectively. We use the observed baryon masses for each channel, and this kinematic factor is also used for the $\Sigma N \to \Lambda N$ transition.

The experimentally obtained $a_{\Lambda N}$ and $r_{\Lambda N}$ of the spin-triplet Λ proton are $a^t_{\Lambda p} = -1.56^{+0.19}_{-0.22}$ fm and $r^t_{\Lambda p} = 3.7^{+0.6}_{-0.6}$ fm, respectively [4]. On the other hand, the Λ-neutron interaction is not measured separately. The sensitivity of the ΛN scattering parameters to the cross section of the reaction will be discussed in Sec. III C.

For the $\Sigma N \to \Lambda N$ transition amplitude $T_{\Sigma N\to\Lambda N}$, we employ the unitarity of S matrix in the isospin-doublet ΛN and ΣN channels. With the diagonal ΛN and ΣN amplitudes given, we determine the off-diagonal amplitude $\Sigma N \to \Lambda N$ according to the unitarity. The details of the calculations are given in the Appendix. The diagonal ΛN and ΣN amplitudes at their threshold are fixed by the scattering lengths. For the ΣN amplitude, we first adopt $a_{\Sigma N} = 1.68 - i2.35$ fm, which is obtained by the Nijmegen NSC97f potential [5]. We also compare the results with $a_{\Sigma N} = -3.83 - i3.01$ fm taken from the Jülich '04 potential [10]. In the following calculations, we introduce the known isospin breaking effect into the transition amplitude $T_{\Sigma N\to\Lambda N}$ through the kinematic factor $\mathcal{N}$ given in Eq. (16). Anyhow the isospin breaking effects on the transition amplitude are irrelevant to the cross sections around the ΛN threshold, because the Σ exchange diagram itself provides little contribution there, as we will see below in the next section.

The $\bar{K}N \to \bar{K}N$, $\bar{K}N \to \pi\Lambda$, and $\bar{K}N \to \pi\Sigma$ amplitudes are given by the chiral unitary model using the parameters in Ref. [54] similarly to Refs. [47–50]. The isospin breaking of these amplitudes is introduced by using the physical hadron masses in the loop functions and kinematic factors of the chiral unitary model. The interaction kernels are given by the Weinberg-Tomozawa interaction and do not contain explicit flavor symmetry breaking. The subtraction constants are also determined in an isospin symmetric way. In Fig. 3, we plot the modules of the $\bar{K}N$ scattering amplitudes used in this work. The isospin breaking of the $\bar{K}N$ thresholds is properly introduced by using the observed masses in the loop functions. It is known that the chiral unitary amplitudes reproduce the observed K^-p scattering cross sections well. (See, for instance, Ref. [57].) Around the $\bar{K}N$ thresholds the isospin breaking effects look large. There, the theoretical description of the $\bar{K}N$ scattering amplitudes could be less reliable. This is because isospin breaking was not considered in the interaction kernels, although the isospin breaking effects may be enhanced around the thresholds.

For $\pi N \to \pi N$ scattering, we use the empirical amplitude $t_{\pi N}$ [60] which is based on the available scattering data. Thus, this amplitude contains certain contributions from the nucleon resonances. It has been constructed isospin symmetrically. Our amplitude $T_{\pi N}$ is obtained by $t_{\pi N}$ with a kinematic factor as follows:

$$T_{\pi N} = -\frac{8\pi M_{\pi N}}{\sqrt{k_i}\sqrt{k_f}\sqrt{2M_i}\sqrt{2M_f}}t_{\pi N}, \tag{17}$$

where $M_{\pi N}$ in the invariant mass of πN, k_i (k_f) is the momentum of the initial (final) pion, and M_i (M_j) is the mass of the initial (final) nucleon. The isospin breaking effect in the πN

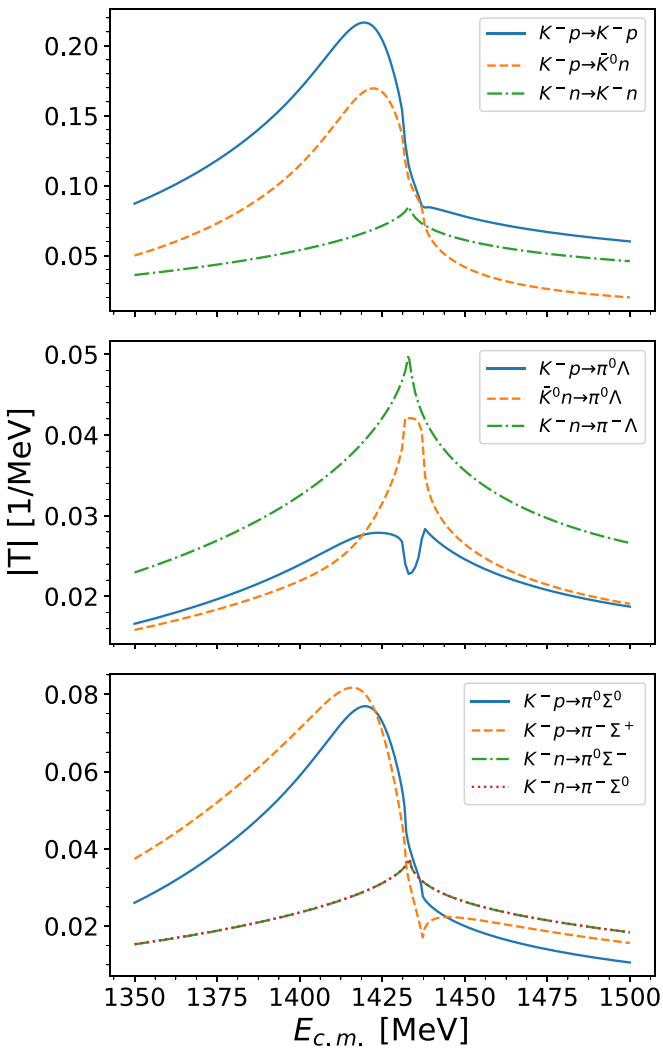

FIG. 3. Modules of $\bar{K}N \to \bar{K}N$, $\bar{K}N \to \pi\Lambda$, and $\bar{K}N \to \pi\Sigma$ scattering amplitude obtained in the chiral unitary approach using the parameters in Ref. [54].

amplitude $T_{\pi N}$ comes from the kinematic factor. We will see below that the contributions of the π exchange are negligibly small, and thus the introduction of the isospin breaking in the πN amplitudes is not important.

III. NUMERICAL RESULTS

In this section, we show numerical results of the calculation for the $K^-d \to \pi^-\Lambda p$ and $K^-d \to \pi^0\Lambda n$ reactions. Using Eq. (1), we evaluate the ΛN invariant mass spectrum as

$$\mathcal{S}_N(M_{\Lambda N}) \equiv k_{\text{c.m.}} \frac{d\sigma}{dM_{\Lambda N}} = \frac{M_d M_\Lambda M_N}{16\pi^3 E_{\text{c.m.}}^2} |\boldsymbol{p}_\pi| \, |\boldsymbol{p}_\Lambda^*| \int |\mathcal{T}_{\pi\Lambda N}|^2 d\cos\theta_\Lambda^* \quad (18)$$

with the $K^-d \to \pi\Lambda N$ scattering amplitude $\mathcal{T}_{\pi\Lambda N}$ discussed in the previous section. In our calculation, the incident kaon momentum in the laboratory frame is fixed at 0 MeV/c.

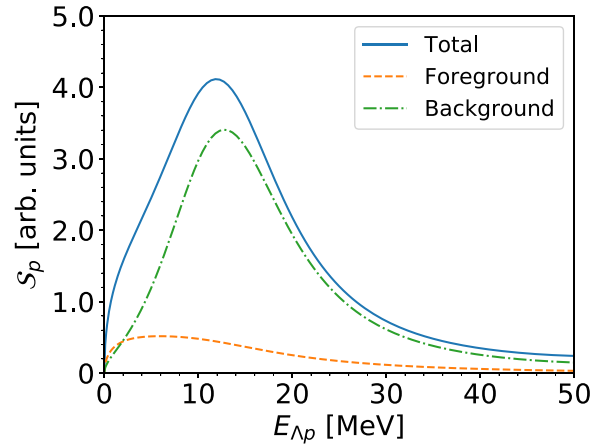

FIG. 4. Λp invariant mass spectrum for the Λp process with stopped kaons. The horizontal axis represents the excitation energy from the threshold in a unit of MeV. The solid, dashed, and dash-dotted lines indicate the contributions of the total amplitudes, the foreground amplitude (only Dia. 1 in Fig. 1), and the background amplitudes (the diagrams other than Dia. 1).

We use the most probable values of the observed spin-triplet Λ-proton scattering parameters $a_{\Lambda p} = -1.56$ fm and $r_{\Lambda p} = 3.7$ fm as the Λ-proton and Λ-neutron scattering amplitudes in Eq. (15), and use $a_{\Sigma N} = 1.68 - i2.35$ (NSC97f).

A. Background reduction

First we discuss background reduction in the ΛN invariant mass spectrum for the $K^-d \to \pi\Lambda N$ reaction. In Fig. 4 we show the Λp invariant mass spectra for the Λp process where θ_Λ^* is integrated from 0 to π. Here we use the excitation energy $E_{\Lambda N}$ defined from the threshold as

$$E_{\Lambda N} \equiv M_{\Lambda N} - (M_\Lambda + M_N) \quad (19)$$

instead of the invariant mass itself. We also plot the separated foreground and background spectra in Fig. 4. As seen in these plots the background contributions dominate the total spectra. Therefore it might be hard to extract the Λp scattering properties from the invariant spectra. We decompose them into components and look for appropriate kinematical conditions to reduce the background contributions.

In Fig. 5, we show the decomposed spectra. As seen in the figure the impulse diagram gives the largest contribution and dominates the background. The contribution from the kaon exchange diagram is the second largest and is comparable with the foreground diagram. The Σ and π exchange diagrams give tiny contributions. Especially the π exchange contribution is found to be negligibly small in the range of the excitation energy.

Let us examine the angular dependence of the cross section for the impulse diagram. With a stopped kaon the final pion is emitted in the opposite direction to the Λ in the laboratory frame, because the initial nucleon in the deuteron has a small Fermi momentum thanks to the small deuteron binding energy. Thus, the impulse diagram gives a larger contribution for larger θ_Λ^*. The kaon exchange diagram has also similar

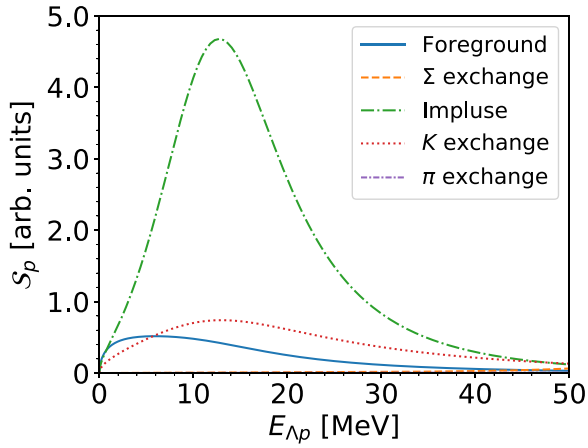

FIG. 5. Decomposed background contributions for the Λp process. The solid, dashed, dash-dotted, dotted, dash-dotted, and short-dash–dotted lines show the contributions from the foreground, Σ exchange, impulse, K exchange, and π exchange diagrams, respectively.

angular dependence because the exchange kaon also has a small momentum for a stopped initial kaon. Therefore, the main background diagrams, Dias. 3 and 4, have a smaller contribution for smaller θ_Λ^*'s. This can be checked by plotting a ratio defined by

$$\mathcal{R}_B = \frac{\left|\mathcal{T}_{\pi\Lambda N}^{\rm BG}\right|^2}{\left|\mathcal{T}_{\pi\Lambda N}^{\rm FG}\right|^2}. \tag{20}$$

As seen in Fig. 6, $\mathcal{R}_B$ is large at $\theta_\Lambda^* > 3\pi/4$. In order to reduce the background, we should avoid this region. In $E_{\Lambda N} \gtrsim 40$ MeV, $\mathcal{R}_B$ is large independently of θ_Λ^*. This is because the contribution of Σ exchange increases as $E_{\Lambda N}$ approaches the ΣN threshold seen in Fig. 5.

In order to reduce the background contributions, let us propose to restrict the integral region of the angle θ_Λ^* as 0 to $\pi/2$. In Fig. 7, we show the total, foreground, and background ΛN mass spectra for the Λp process integrated in the range $[0, \pi/2]$. From Fig. 7, it can be seen that the background contributions are substantially suppressed for $E_{\Lambda p} < 30$ MeV. We also plot the ΛN mass spectrum for each contribution in

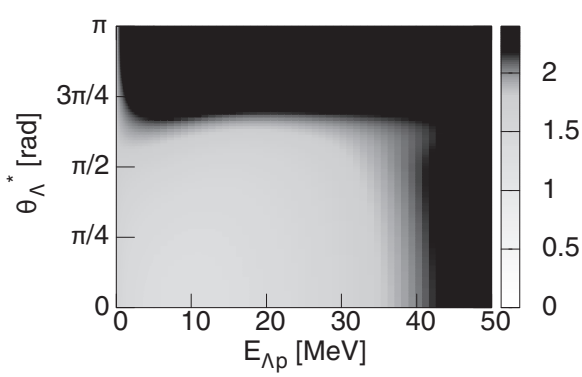

FIG. 6. Two-dimensional plot of $\mathcal{R}_B$ as a function of θ_Λ^* and $E_{\Lambda p}$ for the Λp process.

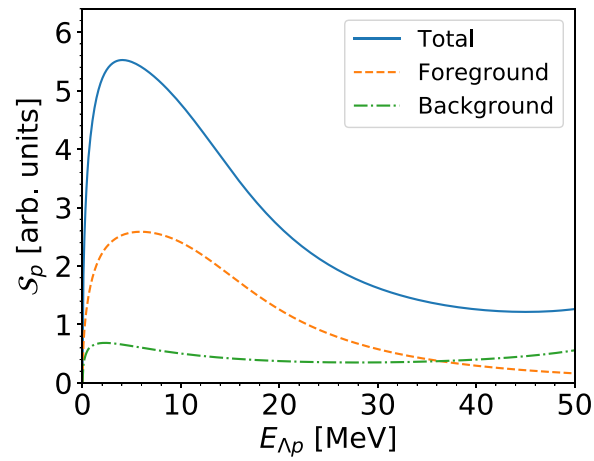

FIG. 7. Λp mass spectrum for the Λp process integrated in the range $[0, \pi/2]$ with stopped kaon. The horizontal axis represents the excitation energy from the threshold in units of MeV. The solid, dashed, and dash-dotted lines indicate the contributions of the total amplitudes, the foreground amplitude (only Dia. 1 in Fig. 1), and the background amplitudes (the diagrams other than Dia. 1).

Fig. 8, showing that the foreground contribution dominates over the other contributions for $E_{\Lambda p} < 40$ MeV. Especially the contribution of the pion exchange diagram is negligibly small. The Σ exchange contribution is also quite small $E_{\Lambda p} < 30$ MeV, but it gets comparable to the foreground contribution for $E_{\Lambda p} > 40$ MeV. Hereafter the integral of θ_Λ^* is performed from 0 up to $\pi/2$.

The purpose of this study is to see isospin symmetry breaking in the ΛN interaction. It is very important to control the isospin symmetry breaking effects from the other sources. In particular, there is a large isospin breaking effect around the $\bar{K}N$ thresholds in the $\bar{K}N \to MB$ amplitudes as seen in Fig. 3. If possible, it is better to avoid these energy region by controlling the kinematical variables of the final state. In the

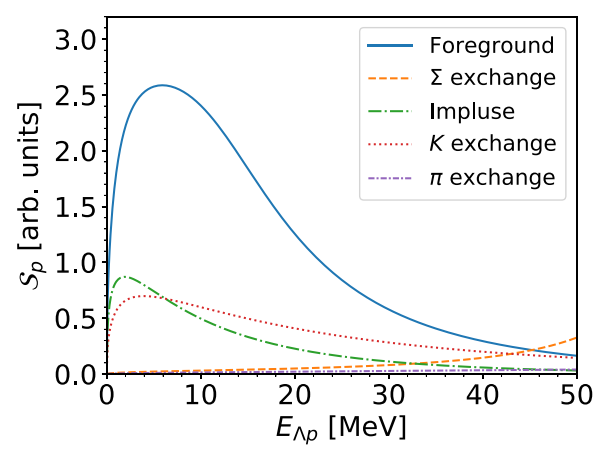

FIG. 8. Decomposed background contributions for the Λp process integrated in the range $[0, \pi/2]$. The solid, dashed, dash-dotted, dotted, dash-dotted, and short-dash–dotted lines show the contributions from the foreground, Σ exchange, impulse, K exchange, and π exchange diagrams, respectively.

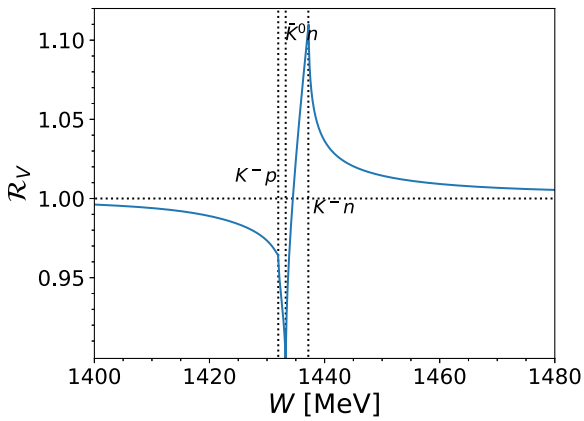

FIG. 9. Ratio (21) for the $\bar{K}N \to \pi\Lambda$ amplitudes as a function of the c.m. energy of $\pi\Lambda$. The thresholds of K^-p, $\bar{K}^0n$, and K^-n are at 1431.95, 1433.24, and 1437.18 MeV, respectively.

diagrams except the impulse approximation (Dia. 3) in Figs. 1 and 2, the energy of the first scattering is determined by those of the initial kaon and the participant nucleon in the deuteron. Thus, the first scattering cannot be controlled by the final state kinematics. For the second scattering, on the other hand, the c.m. energy is dependent on the kinematics of the final state and is controllable.

In order to see isospin breaking of the $\bar{K}N \to \pi\Lambda$ amplitudes, let us plot the following ratio of the $\bar{K}N \to \pi\Lambda$ amplitudes in Fig. 9:

$$\mathcal{R}_V(W) = \frac{|T_{K^-p\to\pi^0\Lambda} - T_{\bar{K}^0n\to\pi^0\Lambda}|}{\sqrt{2}|T_{K^-n\to\pi^-\Lambda}|}. \tag{21}$$

The ratio should be unity if the amplitude is isospin symmetric. This figure shows the large isospin breaking effect around the threshold region, $1420 < W < 1450$ MeV. The c.m. energy of the second scattering is determined by the final state momenta. In order to find kinematic conditions in the final state corresponding a large isospin breaking effect in the $\bar{K}N \to \pi\Lambda$ amplitudes, we show the c.m. energy W of $\pi\Lambda$ as function of θ^*_Λ in Fig. 10 for several $E_{\Lambda p}$. One can see that if one wants to avoid the large isospin breaking

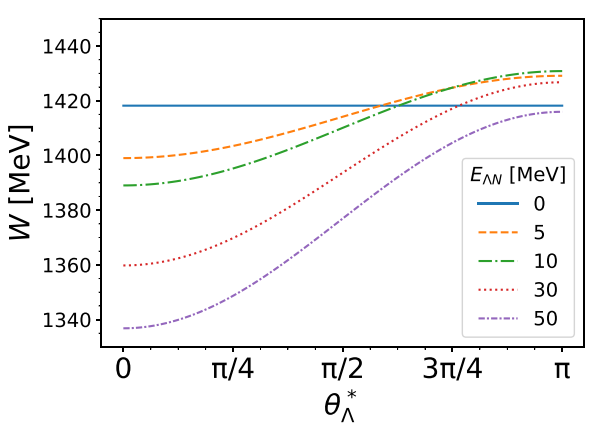

FIG. 10. Center-of-mass energy W of $\pi\Lambda$ as a function of θ^*_Λ for several $E_{\Lambda p}$.

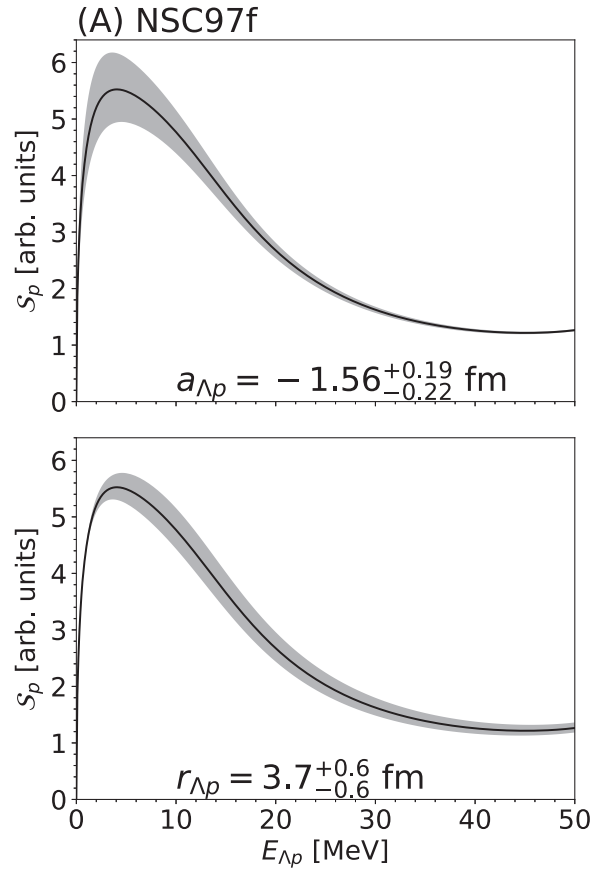

FIG. 11. Λp invariant mass spectra calculated with different $a_{\Lambda p}$ and $r_{\Lambda p}$ values for the Λp process. In the upper plot the value of the scattering length is changed within $a_{\Lambda p} = -1.56^{+0.19}_{-0.22}$ fm, while the value of the effective range varies within $r_{\Lambda p} = 3.7^{+0.6}_{-0.6}$ fm in the lower plot. For the two plots $a_{\Sigma N} = 1.68 - i2.35$ fm (NSC97f) is used.

area $1420 < W < 1450$ MeV for the $\bar{K}N \to \pi\Lambda$ amplitudes, smaller angles are favorable, such as $\theta^*_\Lambda < \pi/2$. This implies that our integral region of θ^*_Λ is in this safe range.

B. Sensitivity to $a_{\Lambda N}$, $r_{\Lambda N}$, and $a_{\Sigma N}$

In this section, we discuss the sensitivity of $a_{\Lambda N}$, $r_{\Lambda N}$, and $a_{\Sigma N}$.

First we evaluate the Λp invariant mass spectra by changing the values of $a_{\Lambda p}$ and $r_{\Lambda p}$ within the experimental errors in order to see the experimental uncertainties on the Λp scattering parameters. The result is shown in Fig. 11 using $a_{\Sigma N} = 1.68 - i2.35$ fm (NSC97f) and Fig. 12 using $a_{\Sigma N} = -3.83 - i3.01$ fm (Jülich '04). In each upper plot we change the value of the scattering length within $a_{\Lambda p} = -1.56^{+0.19}_{-0.22}$ fm with fixing the effective range as $r_{\Lambda p} = 3.7$ fm, while we vary the value of the effective range within $r_{\Lambda p} = 3.7^{+0.6}_{-0.6}$ fm with $a_{\Lambda p} = -1.56$ fm in each lower plot. From these plots one can see that the Λp mass spectrum changes in the regions of the lower excitation energies $0 < E_{\Lambda p} < 15$ MeV when $a_{\Lambda p}$ is varied, and it changes in $5 < E_{\Lambda p} < 30$ MeV when $r_{\Lambda p}$ is varied.

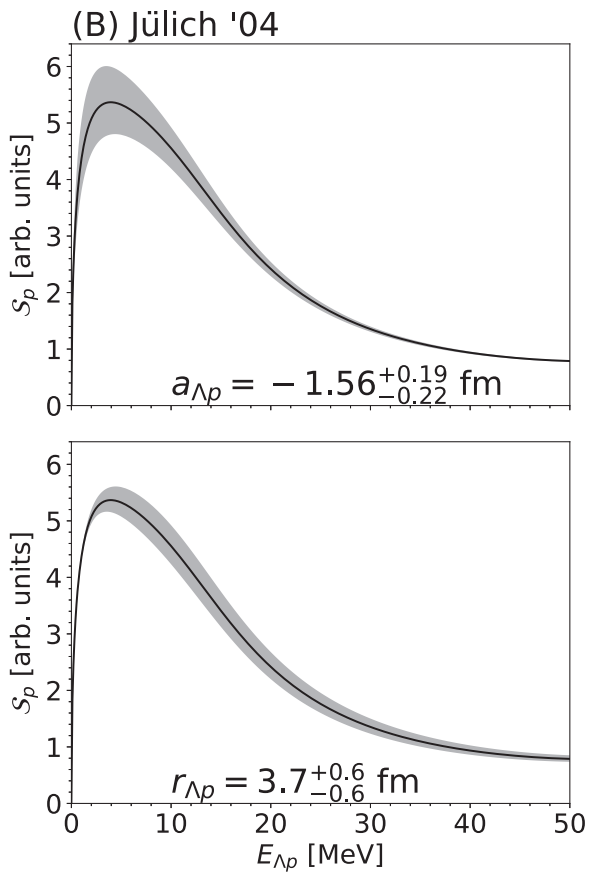

FIG. 12. Same as Fig. 11 but $a_{\Sigma N} = -3.83 - i3.01$ fm (Jülich '04) is used.

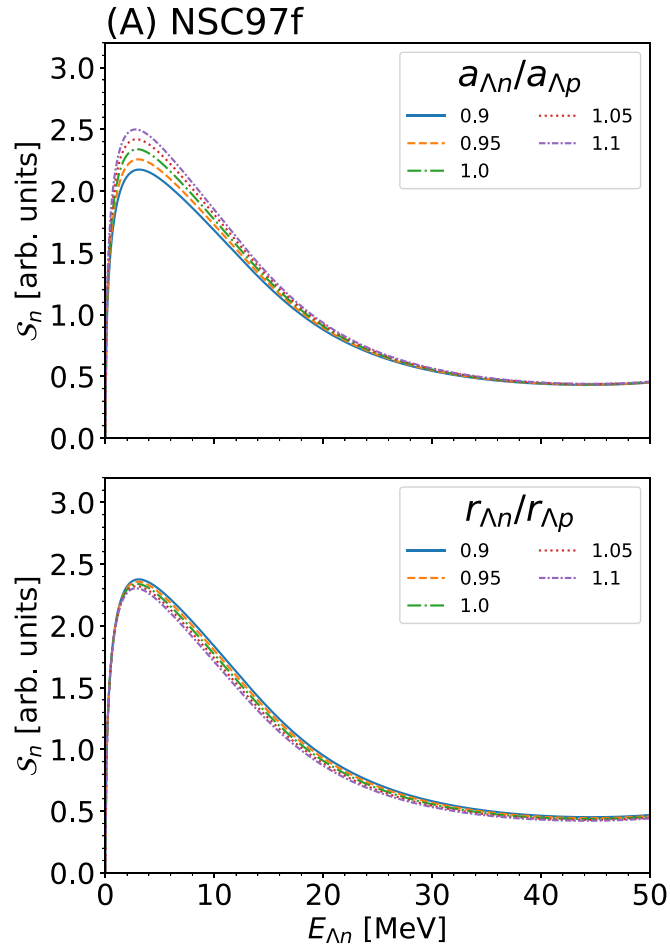

FIG. 13. Λn invariant mass spectra calculated with different $a_{\Lambda n}$ and $r_{\Lambda n}$ values for the Λn process. In the upper plot the value of the scattering length is changed within $\pm 10\%$ of the observed Λp scattering $a_{\Lambda p} = -1.56$ fm, while the value of the effective range varies within $\pm 10\%$ of the observed Λp effective range $r_{\Lambda p} = 3.7$ fm in the lower plot. For the two plots $a_{\Sigma N} = 1.68 - i2.35$ fm (NSC97f) is used.

Comparing Figs. 11 and 12, we find that at low energies the two models have little difference, while at $E_{\Lambda p} > 40$ MeV the spectrum using $a_{\Sigma N} = 1.68 - i2.35$ fm (NSC97f) increases as increase of $E_{\Lambda p}$ and that using $a_{\Sigma N} = -3.83 - i3.01$ fm (Jülich '04) does not.

Next we calculate the invariant mass spectrum for the Λn process. In order to see isospin symmetry breaking, we change the interaction parameters for the Λn process, $a_{\Lambda n}$ and $r_{\Lambda n}$, within $\pm 10\%$ of the experimentally determined values for Λp scattering. In Figs. 13 and 14 we show the calculated spectra with different $a_{\Lambda n}$ and $r_{\Lambda n}$ for the Λn process. In each upper plot we change $a_{\Lambda n}$, while we vary $r_{\Lambda n}$ in each lower plot. One can see from the plots that the invariant mass spectra change significantly in the region $0 < E_{\Lambda n} < 15$ MeV for the scattering length and less significantly in $5 < E_{\Lambda p} < 30$ MeV for the effective range. Again we also compare the results with different a values from NSC97f in Fig. 13 and Jülich '04 in Fig. 14.

One can see that the shapes of the spectra with NSC97f and Jülich '04 are different above 40 MeV, while they are almost the same below 40 MeV. Thus, we could determine the ΛN scattering properties insensitively to the value of $a_{\Sigma N}$ from the invariant mass spectra for $E_{\Lambda N} < 40$ MeV.

C. Ratio between two reactions

It may be difficult to extract the ΛN scattering properties by comparing directly the line shapes of the ΛN invariant mass spectra obtained in experiments to that from the theoretical calculation.

Here we would like to propose to take the ratio of the cross sections as a function of the excitation energy $E_{\Lambda N}$ between the Λn and Λp processes:

$$\mathcal{R}_S = 2\frac{\mathcal{S}_n}{\mathcal{S}_p}, \tag{22}$$

where the factor 2 is introduced to normalize the ratio to be unity when the isospin symmetry is satisfied. Using $\mathcal{R}_S$, we expect to study how different $a_{\Lambda n}$ is from $a_{\Lambda p}$, that is isospin symmetry breaking. We notice that the isospin breaking from other sources is modeled by introducing the observed hadron masses when we calculate the energy-momenta of particles and the kinematic factors. It is also noted that, because the Σ

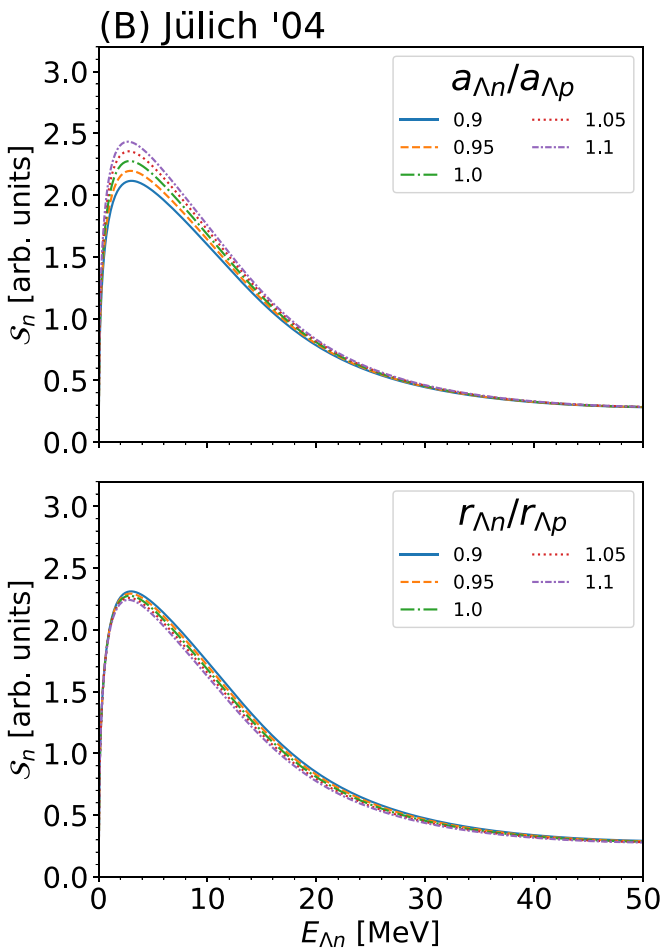

FIG. 14. Same as Fig. 13 but $a_{\Sigma N} = -3.83 - i3.01$ fm (Jülich '04) is used.

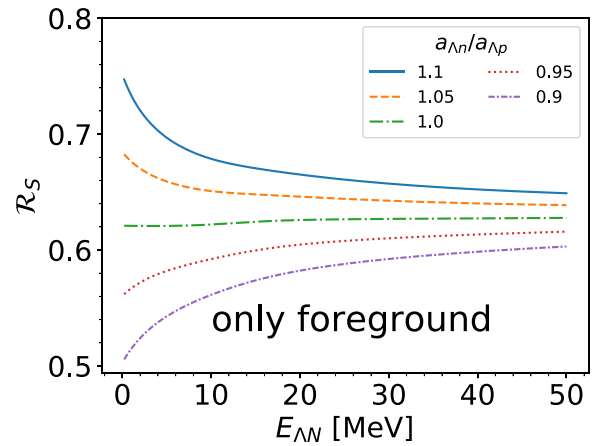

FIG. 15. Ratio $\mathcal{R}_S$ calculated only with the foreground diagram as a function of the excited energy $E_{\Lambda N}$. We take several $a_{\Lambda n}$ values within $\pm 10\%$ of $a_{\Lambda p}$, while the other ΛN parameters are fixed at $a_{\Lambda p} = -1.56$ fm and $r_{\Lambda n} = r_{\Lambda p} = 3.7$ fm.

and π exchange diagrams do not contribute visibly around the ΛN threshold, the isospin breaking in the ΣN transition and πN amplitudes is not important in this calculation.

First of all, we show the ratio calculated only with the foreground diagram in order to check the feasibility of extracting the isospin symmetry breaking effects in the ΛN interaction from $\mathcal{R}_S$. In Fig. 15 we show $\mathcal{R}_S$ for several $a_{\Lambda n}$ values within range of $\pm 10\%$ of $a_{\Lambda p}$. This range must be much wider than the typical uncertainty in the difference between $a_{\Lambda n}$ and $a_{\Lambda p}$ from isospin symmetry breaking. We fix the other ΛN parameters: $a_{\Lambda p} = -1.56$ fm, $r_{\Lambda n} = r_{\Lambda p} = 3.7$ fm. Figure 15 shows that for $a_{\Lambda n}/a_{\Lambda p} < 1.0$ the ratio $\mathcal{R}_S$ tends to go down as the excitation energy approaches the threshold, while for $a_{\Lambda n}/a_{\Lambda p} > 1.0$ it tends to be enhanced. Thus the isospin symmetry breaking effect on the ΛN scattering could be clearly seen, particularly around the threshold if one could observe only the foreground contribution. We find $\mathcal{R}_S$ to work for studying isospin symmetry breaking in the ΛN scattering length. We see that even though $\mathcal{R}_S$ for the isospin symmetric case with $a_{\Lambda n}/a_{\Lambda p} = 1$ is almost constant against the excitation energy, it deviates from unity. This is because of the isospin symmetry breaking of the $K^-N \to \pi\Lambda$ amplitudes (the first scattering in Dia. 1), which is independent of the excitation energy.

Next, we calculate the ratio $\mathcal{R}_S$ by incorporating all the background contributions. We change the Λn scattering length $a_{\Lambda n}$ within $\pm 10\%$ of the Λp scattering length $a_{\Lambda p} = -1.56$ fm and fix the effective range as $r_{\Lambda n} = r_{\Lambda p} = 3.7$ fm again. The results are shown in Fig. 16. The upper panel (in Fig. 16) is calculated with $a_{\Sigma N} = 1.68 - i2.35$ fm (NSC97f) while the lower panel (Fig. 16) is with $a_{\Sigma N} = -3.83 - i3.01$ fm (Jülich '04).

These figures show that the interference to the background contributions gives an enhancement of $\mathcal{R}_S$ at the vicinity of the threshold. Still we find qualitative sensitivity to the change of the ratio $a_{\Lambda n}/a_{\Lambda p}$ in a wide range of the excitation energy, $0 \leqslant E_{\Lambda p} < 30$ MeV, in which the ratio $\mathcal{R}_S$ gets enhanced with larger $a_{\Lambda n}/a_{\Lambda p}$. Unfortunately, we do not find qualitative sensitivity as seen in Fig. 15.

Comparing Figs. 15 and 16, we find that the interference between the foreground and backgrounds is substantially large even if we reduce the background effects by making an angular cut on θ^*_Λ. In order to enhance the interference, we calculate the ratio $\mathcal{R}_S$ without the angular cut. The results are shown in Fig. 17. The difference between $a_{\Lambda n}$ and $a_{\Lambda p}$ can be seen more qualitatively than in Fig. 16. It should be noted that the difference is seen only near threshold up to $E_{\Lambda p} = 10$ MeV. For $a_{\Lambda n}/a_{\Lambda p} < 1.0$, $\mathcal{R}_S$ tends to go down significantly as the excitation energy approaches the threshold, while for $a_{\Lambda n}/a_{\Lambda p} > 1.0$ it tends not to go down so much. This behavior stems from the effect of the interference between the foreground diagram and the impulse diagram, which is the largest background contribution. This will help us to extract the nature of isospin symmetry breaking in the ΛN interaction. At least we could find out the direction of isospin symmetry breaking of the Λn scattering length against Λp.

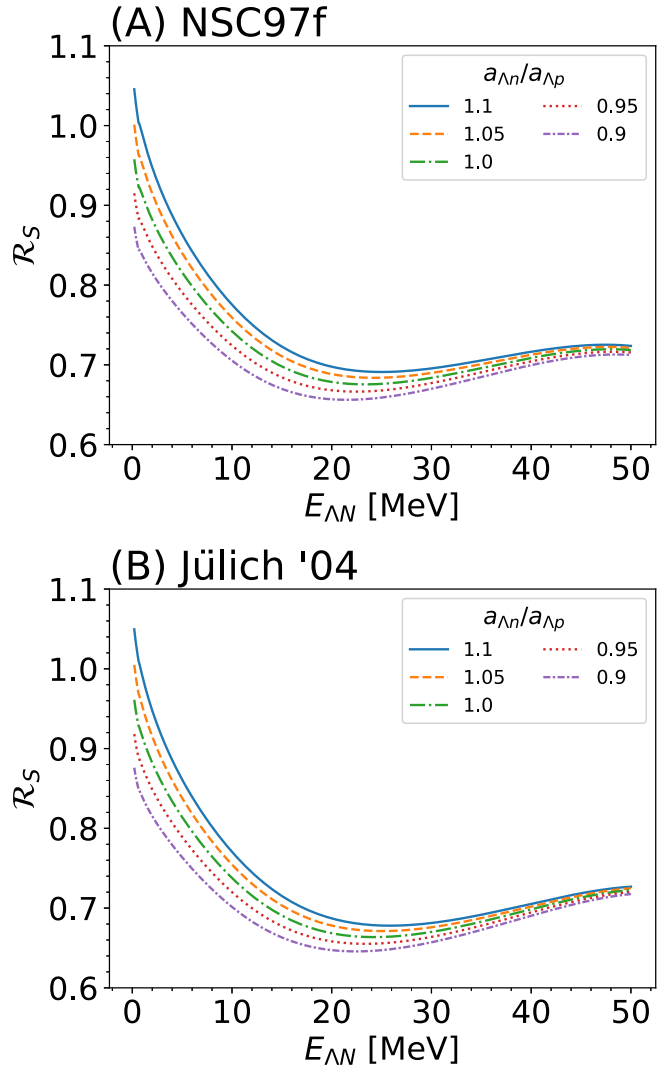

FIG. 16. Same as Fig. 15 but for incorporating the background contributions. The upper and lower panels show the ratios obtained by using the $a_{\Sigma N}$ values in NSC97f and Jülich '04, respectively.

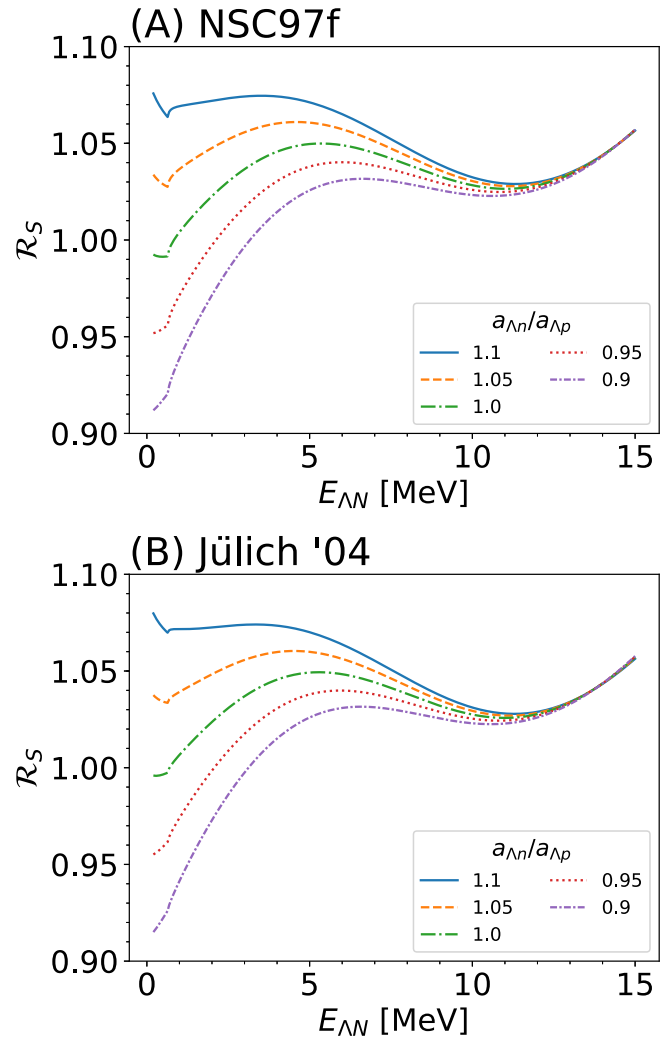

FIG. 17. Same as Fig. 16 but the cutoff of θ_Λ^* is not applied. The upper and lower panels show the ratios obtained by using the $a_{\Sigma N}$ values in NSC97f and Jülich '04, respectively.

D. Comparison to the previous experiments

In order to check the consistency of our formulation with existing experimental data, we compare our calculation with the past experiments of $K^-d \to \pi^-\Lambda p$ with stopped K^-.

First we show the proton kinetic energy T_p spectrum in Fig. 18 together with the experimental data in Ref. [30]. Our calculation is multiplied by a constant to adjust the height to the data. In Ref. [30] the authors showed the kinetic-energy (T_p) distribution of emitted protons in the $K^-d \to \pi^-\Lambda p$ reaction with stopped K^-s as a function of the kinetic energy of the emitted proton, T_p. In their result, a bump structure was found around $T_p = 30$ MeV, but it was not reproduced in the previous theoretical calculation [28]. Reference [30] mentioned that the bump structure would be explained by the effect of the $\Sigma(1385)$ resonance. Nevertheless, it is unnatural that the $\Sigma(1385)$ resonance, coupling to K^-N in the p wave, appears in the relevant energy region of this reaction. Our calculation reproduces nicely the bump structure seen in the experimental data without introducing the $\Sigma(1385)$ resonance. In our calculation, we take into account several diagrams with their interference, and the bump structure is actually explained by the interference between the Σ exchange and other contributions coming from the foreground, the impulse and the kaon exchange diagrams. The theoretical line shown in Ref. [30] considered only the impulse and Σ-Λ conversion effects without their interference. Our calculation shows that one does not have to introduce the $\Sigma(1385)$ resonance in the calculation of such low-energy $\bar{K}N$ scattering.

Next we show the Λp invariant mass spectrum in comparison with the experimental data [31] as plotted in Fig. 19. In Ref. [31] the authors showed the Λp invariant mass distribution in the $K^-d \to \pi^-\Lambda p$ reaction with stopped K^-s. It was pointed out in Refs. [44,45] that only events with proton recoil momenta more than 75 MeV/c were counted in Ref. [31]. Thus, in order to compare our result with the experimental data given in Ref. [31], we make a similar cut on proton momenta in our calculation. Our calculation reproduces well

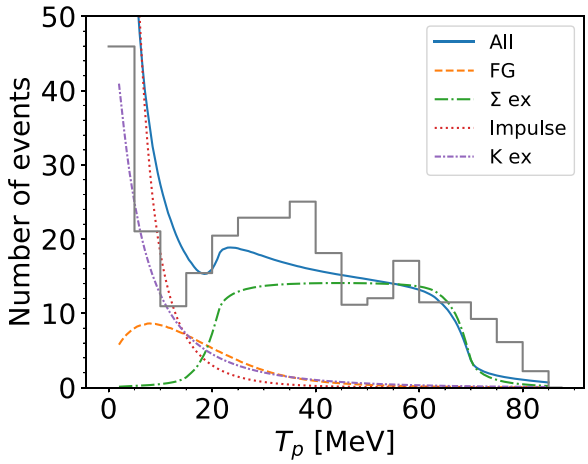

FIG. 18. Proton kinetic energy T_p spectrum for the $K^-d \to \pi^-\Lambda p$ reaction in comparison with the experimental data taken from Ref. [30].

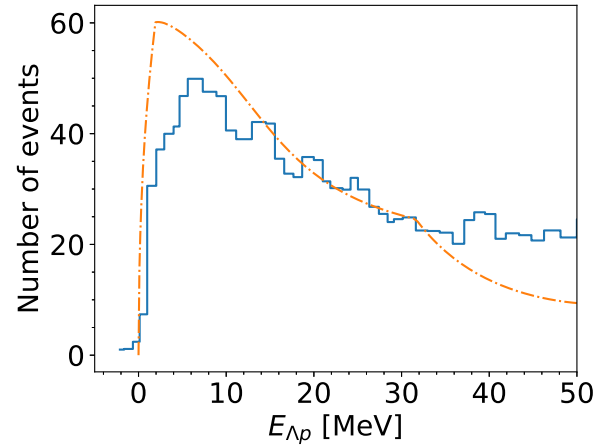

FIG. 19. Λp invariant mass spectrum for the $K^-d \to \pi^-\Lambda p$ reaction in comparison with the experimental data taken from Ref. [31]. The theoretical spectrum is obtained by removing the events with proton momentum less than 75 MeV/c.

the rapid increase at the threshold observed in the experimental data. The Λp invariant mass spectrum without the proton momentum cutoff is shown in Fig. 4.

For future experiments on the $K^-d \to \pi\Lambda N$ reaction, it will be challenging to determine the ΛN invariant mass precisely and accurately. Since neutron detection always involves the uncertainty in estimation of detection efficiency, high resolution is a key issue for energy measurement of neutral pions in the $\pi^0\Lambda n$ final state. It should be noted that the pion energy directly corresponds to the Λn invariant mass when we use stopped kaons. Detecting neutral pions is possible with enough energy resolution for our purpose using the CsI(Tl) calorimeter developed in Refs. [61–63] for instance, which was originally designed for a T-violation search in the $K_{\mu 3}$ decay [64,65]. It is also relatively easy to identify the Λ baryon to confirm the reaction channel of interest through its decay into charged particles. The ΛN invariant mass spectra must be smeared owing to a finite energy resolution, but the energy resolution can be estimated and the smearing effects can be removed by using data obtained with high statistics.

IV. CONCLUSION

In this paper, we have studied $K^-d \to \pi\Lambda N$ reactions with stopped kaons to investigate the difference between low-energy Λp and Λn interactions. We have proposed that the $K^-d \to \pi\Lambda N$ reaction has an advantage for the study of isospin symmetry breaking in the ΛN interaction, because both isospin partners, Λp and Λn, are possible in the final state and we can observe Λp and Λn final state interactions with the same initial condition by selecting the charge of the final state pion. We have formulated the $K^-d \to \pi\Lambda N$ amplitudes by considering not only the foreground contribution which contains the ΛN final state interaction but also background contributions which include the impulse diagram and the Σ, K, and π exchange diagrams. These background diagrams contains the $\pi\Lambda$ and πN final state interactions. For stopped kaons, the ΛN interaction is dominated by the spin triplet configuration because of the deuteron spin and s-wave dominance of low-energy scattering. In order to reduce the background effects, we have examined the dependence of the cross section on the angle between Λ and π in the final state and have found that the background effects can be suppressed for narrower angles between Λ and π.

We have found that the ΛN invariant mass spectra for both the Λp and Λn processes are sensitive to the ΛN scattering properties around the ΛN threshold, $E_{\Lambda p} <$ 30 MeV, and that one may extract the scattering lengths and the effective ranges from these spectra. It has also turned out that the $\Sigma N \to \Lambda N$ transition effect is less important around the ΛN threshold and the π exchange contribution is negligibly small. We have suggested that the ratio of the invariant mass spectra for the Λn and Λp processes works well to extract the qualitative tendency of the charge symmetry breaking effects between the low-energy Λp and Λn scatterings. We have also compared our calculation with the past experiments for $K^-d \to \pi^-\Lambda p$ reaction and found that the calculation reproduces the data well.

ACKNOWLEDGMENTS

The work of Y.I. was partly supported by a Grant-in-Aid for Scientific Research from Japan Society for the Promotion of Science (JSPS) (20J20598). The work of D.J. was partly supported by Grants-in-Aid for Scientific Research from JSPS (17K05449, 21K03530). The work of T.I. was partly supported by Grants-in-Aid for Scientific Research from JSPS (19H01902, 19H05141, 19H05181, 21H00114).

APPENDIX: $\Sigma N \to \Lambda N$ TRANSITION AMPLITUDES

In order to obtain the $\Sigma N \to \Lambda N$ transition amplitude $T_{\Sigma N \to \Lambda N}$, we employ the unitarity of the S matrix in the isospin-doublet ΛN and ΣN channels. The unitarity is implemented to the normalized transition amplitude f, which is defined by $T \equiv \mathcal{N} f$ with the kinematical factor $\mathcal{N}$ given in

TABLE I. Model parameters in units of MeV^{-1}.

$a_{\Sigma N}$	$1.68 - i2.35$ fm (NSC97f)	$-3.83 - i3.01$ fm (Jülich '04)
v_{11}	8.3×10^{-5}	2.1×10^{-2}
v_{12}	6.5×10^{-3}	4.4×10^{-2}
v_{22}	8.8×10^{-3}	7.1×10^{-2}

Eq. (16), as

$$F = (-V^{-1} + iP)^{-1}, \tag{A1}$$

where F, V, and P stand for the matrices of the scattering amplitudes, the interaction kernels, and the momenta, respectively, and are defined as

$$F = \begin{pmatrix} f_{\Lambda N} & f_{\Sigma\Lambda} \\ f_{\Sigma\Lambda} & f_{\Lambda N} \end{pmatrix}, \tag{A2}$$

$$V = \begin{pmatrix} v_{11} & v_{12} \\ v_{12} & v_{22} \end{pmatrix}, \tag{A3}$$

$$P = \begin{pmatrix} p_\Lambda^* & 0 \\ 0 & p_\Sigma^* \end{pmatrix}. \tag{A4}$$

Here, p_Λ^* and p_Σ^* in P are the momenta of Λ and Σ in the Λ-nucleon c.m. frame, respectively. Note that p_Σ^* is pure imaginary when one considers the energy region below the ΣN threshold. Here we assume that model parameters, v_{ij}, are constant.

By using Eq. (A1), we obtain the off-diagonal amplitude $f_{\Sigma N \to \Lambda N}$ from the unitarity of the S matrix. The model parameters are determined so as to reproduce the scattering lengths of the ΛN and ΣN at their thresholds:

$$f_{\Lambda N} = -a_{\Lambda N}, \tag{A5}$$

$$f_{\Sigma N} = -a_{\Sigma N} = -(A - iB) \tag{A6}$$

with the spin-triplet isospin-doublet ΛN scattering length $a_{\Lambda N}$ and ΣN scattering length $a_{\Sigma N} = A - iB$, where A and B are real. We obtain the matrix V:

$$v_{11} = \frac{-\kappa_\Sigma B + a_{\Lambda N}\kappa_\Lambda(1 - \kappa_\Sigma A)}{\kappa_\Lambda(1 - \kappa_\Sigma A + \kappa_\Sigma B a_{\Lambda N}\kappa_\Lambda)}, \tag{A7}$$

$$v_{12} = -\frac{\sqrt{B\left(1 - 2\kappa_\Lambda A + \kappa_\Sigma^2 A^2 + \kappa_\Sigma^2 B^2\right)\left(1 + a_{\Lambda N}^2\kappa_\Lambda^2\right)}}{\sqrt{\kappa_\Lambda}(1 - \kappa_\Sigma A + \kappa a_{\Lambda N} B\kappa_\Lambda)}, \tag{A8}$$

$$v_{22} = \frac{A - \kappa_\Sigma A^2 - \kappa_\Sigma B^2 + a_{\Lambda N} B\kappa_\Lambda}{1 - \kappa_\Sigma A + \kappa_\Sigma a_{\Lambda N} B\kappa_\Lambda}, \tag{A9}$$

where $\kappa_\Lambda = p_\Lambda^*$ at the ΣN threshold and $\kappa_\Sigma = -ip_\Sigma^*$ at the ΛN threshold. All the v_{ij} parameters are real. The determined v_{ij} parameters are summarized in Table I. In these calculation, we use the isospin averaged masses to obtain the kinematical variables and find $\kappa_\Lambda = 283.8$ MeV and $\kappa_\Sigma = 282.6$ MeV.

[1] T. O. Yamamoto *et al.* (J-PARC E13 Collaboration), Phys. Rev. Lett. **115**, 222501 (2015).
[2] A. Esser *et al.* (Mainz A1 Collaboration), Phys. Rev. Lett. **114**, 232501 (2015).
[3] G. A. Miller and W. T. H. V. Oers, Charge independence and charge symmetry, in *Symmetries and Fundamental Interactions in Nuclei* (World Scientific, Singapore, 1995), pp. 127–167.
[4] A. Budzanowski *et al.* (HIRES Collaboration), Phys. Lett. B **687**, 31 (2010).
[5] T. A. Rijken, V. G. J. Stoks, and Y. Yamamoto, Phys. Rev. C **59**, 21 (1999).
[6] T. A. Rijken, M. M. Nagels, and Y. Yamamoto, Prog. Theor. Phys. Suppl. **185**, 14 (2010).
[7] M. M. Nagels, T. A. Rijken, and Y. Yamamoto, Phys. Rev. C **99**, 044003 (2019).
[8] B. Holzenkamp, K. Holinde, and J. Speth, Nucl. Phys. A **500**, 485 (1989).
[9] A. Reuber, K. Holinde, and J. Speth, Nucl. Phys. A **570**, 543 (1994).
[10] J. Haidenbauer and U.-G. Meißner, Phys. Rev. C **72**, 044005 (2005).
[11] K. Tominaga, T. Ueda, M. Yamaguchi, N. Kijima, D. Okamoto, K. Miyagawa, and T. Yamada, Nucl. Phys. A **642**, 483 (1998).
[12] K. Tominaga and T. Ueda, Nucl. Phys. A **693**, 731 (2001).
[13] M. Kohno, Y. Fujiwara, T. Fujita, C. Nakamoto, and Y. Suzuki, Nucl. Phys. A **674**, 229 (2000).
[14] Y. Fujiwara, Y. Suzuki, and C. Nakamoto, Prog. Part. Nucl. Phys. **58**, 439 (2007).
[15] H. Garcilazo, T. Fernandez-Carames, and A. Valcarce, Phys. Rev. C **75**, 034002 (2007).
[16] Y. Fujiwara, C. Nakamoto, and Y. Suzuki, Phys. Rev. C **54**, 2180 (1996).
[17] M. J. Savage and M. B. Wise, Phys. Rev. D **53**, 349 (1996).
[18] C. L. Korpa, A. E. L. Dieperink, and R. G. E. Timmermans, Phys. Rev. C **65**, 015208 (2001).
[19] H. Polinder, J. Haidenbauer, and U.-G. Meißner, Nucl. Phys. A **779**, 244 (2006).
[20] J. Haidenbauer, S. Petschauer, N. Kaiser, U.-G. Meißner, A. Nogga, and W. Weise, Nucl. Phys. A **915**, 24 (2013).
[21] J. Haidenbauer, U.-G. Meißner, and A. Nogga, Eur. Phys. J. A **56**, 91 (2020).
[22] K.-W. Li, X.-L. Ren, L.-S. Geng, and B.-W. Long, Chin. Phys. C **42**, 014105 (2018).
[23] K.-W. Li, X.-L. Ren, L.-S. Geng, and B. Long, Phys. Rev. D **94**, 014029 (2016).
[24] J. Song, K.-W. Li, and L.-S. Geng, Phys. Rev. C **97**, 065201 (2018).
[25] X. L. Ren, E. Epelbaum, and J. Gegelia, Phys. Rev. C **101**, 034001 (2020).
[26] S. Petschauer, J. Haidenbauer, N. Kaiser, U.-G. Meißner, and W. Weise, Front. Phys. **8**, 12 (2020).
[27] J. Haidenbauer, U.-G. Meißner, and A. Nogga, Few-Body Syst. **62**, 105 (2021).
[28] T. Kotani and M. Ross, Nuovo Cimento **14**, 1282 (1959).
[29] T. B. Day and G. A. Snow, Phys. Rev. Lett. **2**, 59 (1959).
[30] O. I. Dahl, N. Horwitz, D. H. Miller, J. J. Murray, and P. G. White, Phys. Rev. Lett. **6**, 142 (1961).

[31] T. H. Tan, Phys. Rev. Lett. **23**, 395 (1969).
[32] D. Cline, R. Laumann, and J. Mapp, Phys. Rev. Lett. **20**, 1452 (1968).
[33] G. Alexander, B. H. Hall, N. Jew, G. Kalmus, and A. Kernan, Phys. Rev. Lett. **22**, 483 (1969).
[34] D. Eastwood, J. R. Fry, F. R. Heathcote, G. S. Islam, D. J. Candlin, G. Copley, G. R. Evans, J. R. Campbell, W. T. Morton, P. J. Negus, M. J. Counihan, D. P. Goyal, D. B. Miller, and B. Schwarzschild, Phys. Rev. D **3**, 2603 (1971).
[35] O. Braun, H. J. Grimm, V. Hepp, H. Strobele, C. Thol, T. J. Thouw, F. Gandini, C. M. Kiesling, D. E. Plane, and W. Wittek, Nucl. Phys. B **124**, 45 (1977).
[36] R. M. A. Fujii, Nuovo Cimento **8**, 643 (1958).
[37] R. Karplus and L. S. Rodberg, Phys. Rev. **115**, 1058 (1959).
[38] A. E. Kudryavtsev, JETP Lett. **14**, 90 (1971).
[39] E. Satoh, Y. Iwamura, and Y. Takahashi, Phys. Rev. Lett. **35**, 1128 (1975).
[40] G. Toker, A. Gal, and J. M. Eisenberg, Phys. Lett. B **88**, 235 (1979).
[41] R. H. Dalitz, C. R. Hemming, and E. J. Morris, Nukleonika **26**, 1555 (1980).
[42] G. Toker, A. Gal, and J. M. Eisenberg, Nucl. Phys. A **362**, 405 (1981).
[43] R. H. Dalitz, Nucl. Phys. A **354**, 101 (1981).
[44] R. H. Dalitz and A. Deloff, Czech J. Phys. B **32**, 1021 (1982).
[45] M. Torres, R. H. Dalitz, and A. Deloff, Phys. Lett. B **174**, 213 (1986).
[46] H. Machner, J. Haidenbauer, F. Hinterberger, A. Magiera, J. A. Niskanen, J. Ritman, and R. Siudak, Nucl. Phys. A **901**, 65 (2013).
[47] D. Jido, E. Oset, and T. Sekihara, Eur. Phys. J. A **42**, 257 (2009).
[48] D. Jido, E. Oset, and T. Sekihara, Eur. Phys. J. A **47**, 42 (2011).
[49] D. Jido, E. Oset, and T. Sekihara, Eur. Phys. J. A **49**, 95 (2013).
[50] J. Yamagata-Sekihara, T. Sekihara, and D. Jido, Prog. Theor. Exp. Phys. **2013**, 043D02 (2013).
[51] N. Kaiser, P. B. Siegel, and W. Weise, Nucl. Phys. A **594**, 325 (1995).
[52] E. Oset and A. Ramos, Nucl. Phys. A **635**, 99 (1998).
[53] M. F. M. Lutz and E. E. Kolomeitsev, Nucl. Phys. A **700**, 193 (2002).
[54] E. Oset, A. Ramos, and C. Bennhold, Phys. Lett. B **527**, 99 (2002); **530**, 260(E) (2002).
[55] T. Hyodo, S. I. Nam, D. Jido, and A. Hosaka, Phys. Rev. C **68**, 018201 (2003).
[56] T. Hyodo, S.-I. Nam, D. Jido, and A. Hosaka, Prog. Theor. Phys. **112**, 73 (2004).
[57] T. Hyodo and D. Jido, Prog. Part. Nucl. Phys. **67**, 55 (2012).
[58] P. A. Zyla *et al.* (Particle Data Group), Prog. Theor. Exp. Phys. **2020**, 083C01 (2020).
[59] R. Machleidt, Phys. Rev. C **63**, 024001 (2001).
[60] SAID partial-wave analysis, available at http://gwdac.phys.gwu.edu/.
[61] D. V. Dementyev *et al.*, Nucl. Instrum. Methods Phys. Res. Sect. A **440**, 151 (2000).
[62] M. Mikhailov and L. Panteleev, Nucl. Instrum. Methods Phys. Res. Sect. A **463**, 288 (2001).
[63] Y. G. Kudenko, Nucl. Instrum. Methods Phys. Res. Sect. A **494**, 318 (2002).
[64] S. Shimizu, K. Horie, M. Abe, M. Aoki, I. Arai, Y. Asano, T. Baker, M. Blecher, M. Chapman, P. Depommier *et al.*, Phys. Lett. B **495**, 33 (2000).
[65] K. Horie, S. Shimizu, M. Abe, M. Aoki, I. Arai, Y. Asano, T. Baker, M. Blecher, M. Chapman, P. Depommier *et al.*, Phys. Lett. B **513**, 311 (2001).